

Baryons, Neutrinos, Feedback and Weak Gravitational Lensing

Joachim Harnois-Déraps^{1,2*}, Ludovic van Waerbeke¹, Massimo Viola³, Catherine Heymans⁴

¹*Department of Physics and Astronomy, University of British Columbia, V6T 1Z1, B.C., Canada*

²*Canadian Institute for Theoretical Astrophysics, University of Toronto, M5S 3H8, On., Canada*

³*Leiden Observatory, Leiden University, PO Box 9513, NL-2300 RA Leiden, Netherlands*

⁴*Scottish Universities Physics Alliance, Institute for Astronomy, University of Edinburgh, Royal Observatory, Blackford Hill, Edinburgh, EH9 3HJ, UK*

9 October 2018

ABSTRACT

The effect of baryonic feedback on the dark matter mass distribution is generally considered to be a nuisance to weak gravitational lensing. Measurements of cosmological parameters are affected as feedback alters the cosmic shear signal on angular scales smaller than a few arcminutes. Recent progress on the numerical modelling of baryon physics has shown that this effect could be so large that, rather than being a nuisance, the effect can be constrained with current weak lensing surveys, hence providing an alternative astrophysical insight on one of the most challenging questions of galaxy formation. In order to perform our analysis, we construct an analytic fitting formula that describes the effect of the baryons on the mass power spectrum. This fitting formula is based on three scenarios of the OWL hydrodynamical simulations. It is specifically calibrated for $z < 1.5$, where it models the simulations to an accuracy that is better than 2% for scales $k < 10h\text{Mpc}^{-1}$ and better than 5% for $10 < k < 100h\text{Mpc}^{-1}$. Equipped with this precise tool, this paper presents the first constraint on baryonic feedback models using gravitational lensing data, from the Canada France Hawaii Telescope Lensing Survey (CFHTLenS). In this analysis, we show that the effect of neutrino mass on the mass power spectrum is degenerate with the baryonic feedback at small angular scales and cannot be ignored. Assuming a cosmology precision fixed by WMAP9, we find that a universe with no baryon feedback and massless neutrinos is rejected by the CFHTLenS lensing data with 96% confidence. Some combinations of feedback and neutrino masses are also disfavoured by the data, although it is not yet possible to isolate a unique neutrino mass and feedback model. Our study shows that ongoing weak gravitational lensing surveys (KiDS, HSC and DES) will offer a unique opportunity to probe the physics of baryons at galactic scales, in addition to the expected constraints on the total neutrino mass.

Key words: cosmology: cosmological parameters — dark matter — gravitational lensing: weak lensing — galaxies: formation — neutrinos

1 INTRODUCTION

Recent results from the Canada France Hawaii Telescope Lensing survey (CFHTLenS), a stage II survey (Albrecht et al. 2006), has demonstrated the power of weak gravitational lensing to probe cosmology (Benjamin et al. 2013; Simpson et al. 2013; Kilbinger et al. 2013; Heymans et al. 2013; Kitching et al. 2014; Fu et al. 2014). While stage III surveys are currently ongoing (de Jong et al. 2013; Sánchez & DES Collaboration 2014), significant effort is underway in order to reach the precision required by stage IV weak lensing surveys, with the series of GREAT challenges (Mandelbaum et al. 2014) devoted to shape measurement, for instance. A better understanding of the lensing signal at small

scales is also necessary and this relies on high resolution numerical simulations.

It is known that at small angles smaller (e.g., scales smaller than half a degree, for sources at $z_s \sim 0.5$) the lensing signal suffers from a large number of theoretical uncertainties: non-linear clustering, projection effects, baryonic physics to name just a few. On the other hand, the precision of standard big-bang cosmological parameters has improved considerably during the last decade thanks to wide field surveys probing background cosmology (see Weinberg et al. 2013, and references therein for a review). The situation today is that our knowledge of most cosmological parameters greatly surpasses our knowledge of the physics of groups and clusters of galaxies. For instance, the mean mass density of the Universe is known to better than 3.5% (Hinshaw et al. 2013; Planck Collaboration et al. 2013), which corresponds to a $\sim 6\%$ uncertainty in the mass power spectrum. On the other hand, the uncer-

* E-mail: jharno@cita.utoronto.ca

tainty caused by different Active Galactic Nuclei (AGN) feedback models could be as large as 50% for physical scales $k < 1h\text{Mpc}^{-1}$ (van Daalen et al. 2014). This could be particularly problematic for current and future weak lensing surveys since the majority of the signal-to-noise comes from small angular scales (Semboloni et al. 2011), and that in order to measure the dark energy equation of state, it would help considerably to be able to utilize these scales. The other alternative is to restrict lensing analysis to physical scales where these problems are minimized or disappear (Kitching et al. 2014), or to treat the problematic scales as a nuisance that should be marginalized over (Eifler et al. 2014).

The approach we take in this paper relies on two facts: 1) if all the matter was dark matter, the non-linear clustering would be known very accurately from numerical simulations (Heitmann et al. 2013; Harnois-Déraps & van Waerbeke 2014) and 2) most relevant background cosmological parameters are known to 1–2 percent (Hinshaw et al. 2013; Planck Collaboration et al. 2013). One can therefore assume a fixed cosmology and quantify how strongly the data deviate from the pure dark matter scenario. This deviation can then be compared to various hydrodynamic simulations implementing different models of baryonic feedback, treating the residual uncertainty in the assumed cosmology as a systematic error in this comparison.

The neutrino mass is the only background cosmology parameter that is not known with great precision and yet, it is very important for our study. Riemer-Sørensen et al. (2012) and Zhao et al. (2013) have measured upper bounds for the neutrino mass, but these studies also show that the modelling at small scales $k > 0.5h\text{Mpc}^{-1}$ is an issue with redshift surveys. As shown in Rossi (2014), in the context of the Lyman-Alpha forest, the neutrino mass is best constrained by combining small and large physical scales; this is why gravitational lensing is one of the best approaches for this type of measurement (Cooray 1999), in particular because the level of modelling at small scales is less complicated than for redshift surveys. Recent attempts at constraining the neutrino mass by combining CFHTLenS measurements with other cosmology probes suggest that the technique is promising (Beutler et al. 2014; Battye & Moss 2014). Unfortunately, the new developments on the role of AGN feedback show that even with gravitational lensing, baryonic physics has an important effect at small scales. It has been shown recently that the neutrino mass and baryonic feedback are relatively degenerate (Natarajan et al. 2014). Our strategy in this paper is therefore to explore the combined effect of different baryonic feedback models and neutrino masses on gravitational lensing measurements, assuming that the background cosmology is known to sufficient accuracy. For this purpose we derive a fitting formula for some specific baryonic feedback models that can be used to predict the matter power spectrum at all scales and redshifts.

In Section 2, we briefly review the theoretical background relevant for cosmic shear measurements, we describe our different prediction models and present a convenient fitting function for different baryon feedback processes. We present the data, the simulations and the measurements in Section 3, and discuss the results and conclude in Section 4. We assume a fiducial cosmology for our simulations and models based on a the WMAP9+BAO+SN ΛCDM best fit parameters, namely $(\Omega_\Lambda, \Omega_M, \Omega_b, n_s, A_s, h) = (0.7095, 0.2905, 0.0473, 0.969, 2.442 \times 10^{-9}, 0.6898)$. For a zero neutrino mass, the value of σ_8 in this fiducial model is 0.831. This number is calculated from A_s for each neutrino mass tested in this analysis. The reason for choosing the WMAP9 cosmology as our baseline (as opposed to a Planck cosmology) roots in a known tension between the Planck and CFHTLenS results

(Planck Collaboration et al. 2013), which could have biased our analysis towards an over-rejection of theoretical models (see Section for more details).

2 BACKGROUND

2.1 Theory

The dark matter power spectrum $P(k)$ is extracted from the dark matter overdensity fields $\delta(\mathbf{x})$ by :

$$\langle |\delta(\mathbf{k})\delta(\mathbf{k}')| \rangle = (2\pi)^3 P(\mathbf{k})\delta_D^3(\mathbf{k}' - \mathbf{k}) \quad (1)$$

where $\delta(\mathbf{k})$ is the Fourier transform of $\delta(\mathbf{x})$, and $P(k)$ is obtained by averaging $P(\mathbf{k})$ over all directions. Under the Limber approximation (Limber 1954), the weak lensing power spectrum C_ℓ^k is related to matter power spectrum with:

$$C_\ell^k = \frac{1}{\ell} \int_0^\infty dk W^2(\ell/k) P(k, z), \quad W(\chi) = \frac{3H_0^2 \Omega_M}{2c^2} \chi g(\chi) (1+z) \quad (2)$$

where $\ell = \chi k$, c is the speed of light, H_0 the Hubble parameter, Ω_M the mean matter density in units of critical density, χ the comoving distance to the observer and $g(\chi)$ describes the lensing geometry of the system, with a source redshift distribution $n(z)$:

$$g(\chi) = \int_\chi^{\chi_H} n(\chi') \frac{\chi' - \chi}{\chi'} d\chi' \quad (3)$$

The cosmic shear correlation functions $\xi_\pm(\theta)$ are computed from this quantity with:

$$\xi_\pm(\theta) = \frac{1}{2\pi} \int C_\ell^k J_{0/4}(\ell\theta) \ell d\ell \quad (4)$$

where $J_{0/4}(x)$ are Bessel functions.

2.2 Models of $P(k)$

2.2.1 Dark matter only models

Although the largest scales of the matter field can be accurately described by linear perturbation theory, the smallest scales require modelling of the non-linear regime of gravitational collapse. The weak lensing measurements we analyze in this work extend down to sub-arcminute scales, hence it is necessary to include scales up to $k = 40h\text{Mpc}^{-1}$ in the model predictions. These are very deep into the non-linear regime, where the modelling is not fully tested, thereby it is essential to quantify the theoretical uncertainties. Our approach is to assume a fixed, fiducial cosmology, compare a series of theoretical predictions for $P(k)$, and estimate the error on the theory as the scatter across the models (see Table 1 for a list of the models considered in this work).

HF2 model: The power spectrum from the widely used HALOFIT (Smith et al. 2003) fitting function including its recalibration by Takahashi et al. (2012). Known limitations include 5–10 percent over-prediction of power for $0.5 < k < 5h\text{Mpc}^{-1}$ in standard ΛCDM cosmology (Heitmann et al. 2010), mainly due to a coarse sampling of the cosmological parameter space. Smaller scales deviate from other models, hence we consider this model to be 10 percent accurate.

CEHF model: An alternative to universal fitting functions has been proposed by Heitmann et al. (2010), which instead interpolate the power spectrum from an ensemble of well-controlled N -body simulations. This Cosmic Emulator has been shown to

be accurate at the percent level up to $k = 1h\text{Mpc}^{-1}$ and 5 percent up to $k = 10h\text{Mpc}^{-1}$ (Heitmann et al. 2013). Smaller scales are not available with the Cosmic Emulator, which is unfortunate for weak lensing studies since these scales contribute significantly to the shear correlation functions at the arcminute level (Harnois-Deraps & van Waerbeke 2014). Following Eifler (2011), we extend the Cosmic Emulator at smaller scales by grafting the HF2 predictions, with an overall normalization factor to ensure continuity across the junction. The grafted scales are considered to be 10 percent accurate.

CEP model: By construction, the CEHF model reproduces the same shape as HF2 at small scales, which is not guaranteed to be accurate. We therefore devise another empirical model in which the Cosmic Emulator is extrapolated to smaller scales by a simple power law, fit over the range $5 < k < 10h\text{Mpc}^{-1}$, and then extended to $k = 40h\text{Mpc}^{-1}$. When compared with high resolution simulations (see the HR model below), we find that a function of the form

$$P^{CEP}(k) \propto k^{\alpha(z)-3.0}, \quad k > 10h\text{Mpc}^{-1} \quad (5)$$

with $\alpha(z) = 0.92(1+z)^{0.1}$ provides a smooth and precise extrapolation for $z \leq 2$. The proportionality constant is simply found by matching the amplitude at $k = 10h\text{Mpc}^{-1}$. We note that higher redshifts are better described with higher values for α than those prescribed here (up to 25 percent higher by $z = 3$). Given the redshift distribution for our sample of CFHTLenS galaxies has a mean redshift $< z_s > \sim 0.9$ (see Section 3.1), this correction on α has negligible effect on our measurement. Compared to CEHF, this model has the extra advantage that its derivative is continuous, which is desired for most Fisher matrix calculations. The accuracy of the grafted scales are taken to be 10 percent up to $k = 20h\text{Mpc}^{-1}$, and 20 percent for smaller scales, to be conservative.

HF1b model: Before the recalibration by Takahashi et al. (2012), the HALOFIT model (HF1) was under predicting the small scale power by up to a factor of two (Heitmann et al. 2010). However, an analytical rescaling of the original (Smith et al. 2003) predictions, proposed by John Peacock¹, was found to reproduce with high fidelity the results from high resolution N -body simulations. This model can be constructed from HALOFIT (< 2012 versions) as:

$$P^{HF1b}(k) = \left[P^{HF1}(k) - P_{lin}(k) \right] \times \frac{1 + 2y^2}{1 + y^2} + P_{lin}(k) \quad (6)$$

where $y = k/(10h\text{Mpc}^{-1})$. As a result, HF1b is considered in this work, but not HF1, and the accuracy is taken to be 10 percent for $0.1 < k < 1h\text{Mpc}^{-1}$, 15 percent for $k > 1h\text{Mpc}^{-1}$, and 5 percent at smaller k -modes.

HR model: Our last candidate for $P(k)$ is taken from a recent N -body simulation suite, the Scinet Light Cone Simulations (SLICS), which achieve a precision better than five percent for scales of $k < 30h\text{Mpc}^{-1}$ in the high resolution series. Features of the SLICS series are summarized in Section 3.2 and detailed in Harnois-Deraps & van Waerbeke (2014, HDVW hereafter). This is not a model *per se* but a measurement estimated from light cone simulations created with an independent N -body code; it is therefore an important indicator of the level of precision that is achievable. We treat the HR model as an additional estimate of the signal, with five percent accuracy to $k < 10h\text{Mpc}^{-1}$, 10 percent accuracy to $k = 20h\text{Mpc}^{-1}$ and 20 percent accuracy to $k = 30h\text{Mpc}^{-1}$. For $k > 30h\text{Mpc}^{-1}$, the model is considered to be precise to within

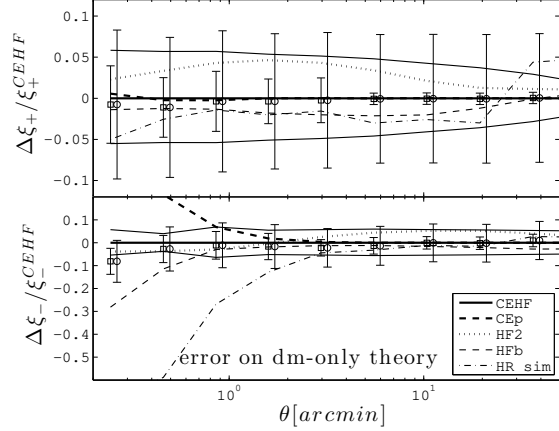


Figure 1. Fractional error on the dark matter only theoretical models for shear correlation functions ξ_+ (top) and ξ_- (bottom). Results are compared to the CEHF model. Squares with error bars are the weighted mean and error across the different models (see the main text for details about the variance on individual models). The upper (lower) thin solid lines in each panel correspond to the effect of a 1σ upward (downward) fluctuation in Ω_M on the CEHF model, compared to the baseline cosmology. The open circles (slightly shifted for clarity) represent the same weighted mean, but the larger error bars combine in quadrature the theoretical error on the dark matter model and the uncertainty on Ω_M .

a factor of two, effectively downweighting the regions that suffer from limitations due to mass resolution in the N -body calculation.

For each of these dark-matter only models, we compute the shear correlation functions ξ_{\pm} and report the result in Fig. 1, organized as fractional difference with respect to the CEHF model. The agreement between the different ξ_+ models is at the level of a few percent even at 0.3 arcminutes. We find HF2 to be the main outlier. Models of ξ_- achieve the same level of accuracy down to about 3 arcminutes, but smaller angles do not reach the same level of agreement. The squares with error bars in Fig. 1 are the weighted mean and error (1σ) across models, obtained by weighting each model by its inverse variance. Overall, we achieve a 1 percent precision on ξ_+ for angles larger than $5'$, and a 4 percent precision for smaller angles. The precision on ξ_- is poorer as this quantity is probing deeper into the non-linear regime: we achieve four percent precision on angles larger than $3'$, and an eight percent precision for smaller angles. Recall that this is the error on the non-linear weak lensing signal for a fixed cosmology universe in which there is no baryonic feedback nor massive neutrinos.

We also show in the figure the effect on the CEHF model of a 1σ fluctuation in Ω_M compared to the fiducial value. The open circles with larger error bars show the combined (model + cosmology) uncertainty, as fully described in Section 3.4.4.

2.2.2 Neutrino feedback

The effect of the neutrino free-streaming on the dark matter structure has been calculated from simulations with a high level of precision and incorporated into the CAMB cosmological code (Lewis et al. 2000; Bird et al. 2012) with less than 10 percent error at $k = 10h\text{Mpc}^{-1}$. With this tool, we compute the mass power spectrum for our model with both dark matter and massive neutrinos, $P_{HF2}^{DM+\nu}(k)$, assuming one massive and two massless flavours. We explore three different total neutrino masses M_ν of 0.2, 0.4, and 0.6 eV in addition to the massless case $M_\nu = 0$. The ratio between

¹ www.roe.ac.uk/~jap/hafoes

these and the dark matter only model provide our four predictions of the *neutrino feedback bias*:

$$b_{M_\nu}^2(k, z) \equiv \frac{P^{DM+M_\nu}(k, z)}{P^{DM}(k, z)}, \quad (7)$$

where the M_ν superscript specifies the total neutrino mass considered. For each model X of Table 1, we implement the neutrino feedback with a multiplicative bias factor, i.e. $P_X^{DM+\nu} = P_X^{DM} \times b_{M_\nu}^2$, with $X = (\text{HF2}, \text{HF1b}, \dots)$.

2.2.3 Baryon feedback

The baryonic feedback models are obtained² from a subset of the hydrodynamical simulation suite ran in the context of the Over-Whelmingly Large (OWL) Simulation Project (Schaye et al. 2010). The dark matter density fields of these simulations were compared to a dark matter only baseline, and discrepancies were reported as baryonic feedback on the dark matter (van Daalen et al. 2011). Amongst different models, we selected four models: 1) the dark matter only (DM-ONLY) 2) the reference baryonic model (REF) that describes prescriptions for cooling, heating, star formation and evolution, chemical enrichment and supernovae feedback and 3) a model that has an additional contribution from the active galactic nuclei feedback (AGN), and 4) a top-heavy stellar initial mass function (DBLIM), but no AGN feedback (see van Daalen et al. 2011, for details about these simulations). Following van Daalen et al. (2011); Semboloni et al. (2011), we model the baryonic feedback on dark matter by taking the ratio with the DM-ONLY model, and define the *baryon feedback bias* as:

$$b_m^2(k, z) \equiv \frac{P_{\text{OWL}}^{DM+b(m)}(k, z)}{P_{\text{OWL}}^{DM}(k, z)}, \quad (8)$$

where the index $b(m)$ runs over the different baryon feedback models (AGN, REF, ...), and the subscript OWL specifies that these quantities are measured from the OWL simulation suite. The lower section of Table 1 summarizes the baryonic feedback models considered in this paper.

2.2.4 Combined feedback

In this analysis, we consider all combinations of the four neutrino masses (three with $M_\nu > 0$, plus the massless case) with the four baryon feedback models (three with baryonic physics, plus the no baryon case) for a total of 16 models, all constructed from:

$$P^{DM+\nu+b(m)}(k, z) = P^{DM}(k, z) \times b_m^2(k, z) \times b_{M_\nu}^2(k, z) \quad (9)$$

The underlying assumption from this ‘multiplicative’ parameterization is that the baryonic feedback is independent of the neutrino free streaming. This statement is justified since Bird et al. (2012) found that baryons have a one percent effect on the neutrinos for $k < 8h\text{Mpc}^{-1}$ with a gradual increase at smaller scales. This is clearly subdominant compared to the baryon feedback itself, reinforcing the validity of our multiplicative feedback method.

The left panels of Fig. 2 illustrate the action of different combinations of baryons and massive neutrinos on the dark matter power spectrum. The right panels show the same combinations propagated on the weak lensing power spectrum C_ℓ^k with equation 2. As noted by Natarajan et al. (2014), the two sources of feedback are highly degenerate for $\ell > 1000$ and will be challenging to distinguish in

Table 1. The theoretical models considered in this paper. The Cosmic Emulator (CE) has a small scale k -cut at $10.0h\text{Mpc}^{-1}$, which affects many scales relevant for the current studies. As described in the main text, we therefore extend the CE to smaller scales by grafting either the HALOFIT2012 predictions (CEHF model) or a power law (CEp model). References for these models are also provided in the main text.

Description	k -modes included [in $h\text{Mpc}^{-1}$]	Name
HALOFIT2012	$0.001 < k < 40.0$	HF2
HALOFIT2011 ‘corrected’	$0.001 < k < 40.0$	HF1b
Cosmic Emulator	$0.001 < k < 10.0$	CEHF
+ HALOFIT 2012 extension	$10.0 < k < 40.0$	
Cosmic Emulator	$0.001 < k < 10.0$	CEp
+ Power law extension	$10.0 < k < 40.0$	
Large ensemble suite ($N_{\text{sim}} = 500$)	$0.0124 < k < 20.0$	SLICS-LE
High resolution suite ($N_{\text{sim}} = 5$)	$0.0124 < k < 20.0$	SLICS-HR
Dark matter baseline for baryons	$0.0013 < k < 100.0$	dm-only
Reference for baryonic feedback	$0.0013 < k < 100.0$	REF
REF + AGN feedback	$0.0013 < k < 100.0$	AGN
REF + top-heavy IMF	$0.0013 < k < 100.0$	DBLIM

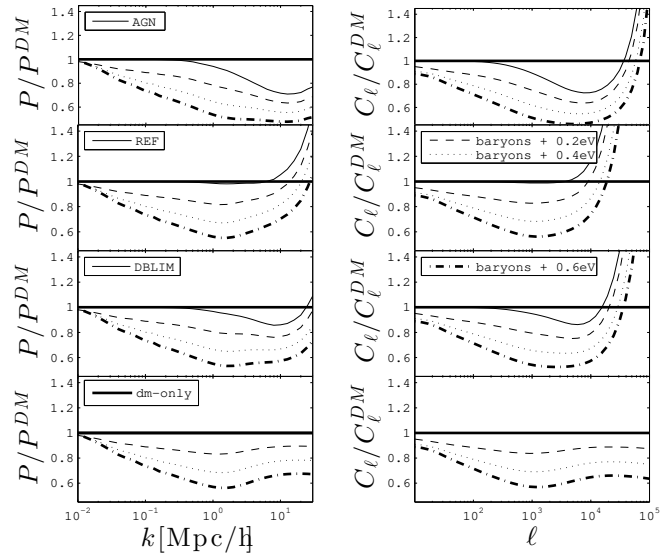


Figure 2. (Left:) Combined feedback from baryons and massive neutrinos on the dark matter power spectrum, measured at $z = 0.042$. Each panel shows the dark matter only model as the thick horizontal line, and the dark matter + baryons as the thin solid line. Top to bottom are AGN, REF, DBLIM and DM-ONLY baryon models respectively. Also shown is the impact of neutrinos on each model, shown as thin dashed lines (0.2eV), dotted lines (0.4eV), and thick dash-dotted lines (0.6eV). (Right:) Same as the left panel, but for the weak lensing power spectra, assuming the source redshift distribution given by equation 11.

coming surveys. The region with $\ell < 1000$ is more sensitive to neutrino masses and could break the degeneracy, although it is more affected by sampling variance. The optimal choice will be affected by the mean source redshift and the noise level, and will therefore differ slightly in each survey.

² OWL simulations: <http://vd11.strw.leidenuniv.nl/>

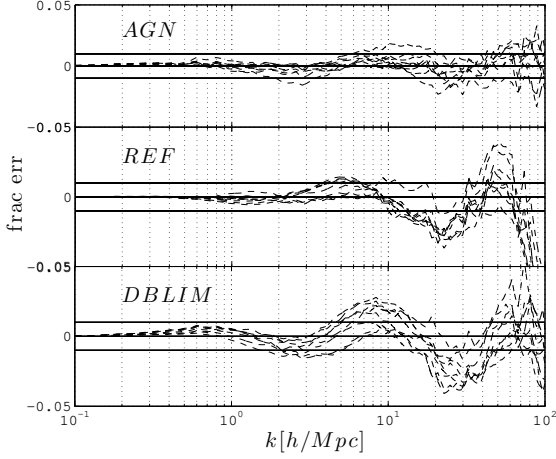


Figure 3. Fractional error between the baryon bias fit function (equation 10) and that measured by van Daalen et al. (2011). The horizontal lines highlight the 1 percent error. Each panel contains the result for 8 different redshifts in the range $0 \leq z \leq 1.5$. Higher redshifts show stronger errors, as mentioned in the text. Nevertheless, the fit still describes the bias with sub percent level precision up to $k \sim 1h\text{Mpc}^{-1}$ and better than 10 percent precision up to $k \sim 20h\text{Mpc}^{-1}$. Smaller scales contribute negligibly to the cosmic shear signal, unless probing deep in the sub-arcminute regime.

2.3 Fitting formula for baryon feedback

Whilst massive neutrinos are already featured in CAMB’s mass power spectrum predictions, baryon feedback, however, is not included. For this purpose, we provide a fitting function for the three baryonic feedback models considered here (REF, DBLIM and AGN). For each model, our fitting function is designed to reproduce the baryonic effects on the total mass power spectrum for any redshift and scale with high precision. It can then easily be incorporated to CAMB or any other tool to create fully non-linear power spectrum predictions that include baryonic effects.

For the three feedback models considered here, we find that the baryon feedback bias is well described by the following functional form:

$$b_m^2(k, z) = 1 - A_z e^{(B_z x - C_z)^3} + D_z x e^{E_z x} \quad (10)$$

with $x = \log_{10}(k/[h\text{Mpc}^{-1}])$. The five terms A_z , B_z , C_z , D_z and E_z depend on redshift, closely following a quadratic polynomial in powers of the scale factor, i.e. $A_z = A_2 a^2 + A_1 a + A_0$, with $a = 1/(1+z)$. The best fit parameters for each model are presented in Table 2, and compared to a direct interpolation from the measurements of van Daalen et al. (2011) in Fig. 3, for $z < 1.5$. We see that this parameterization is accurate at the sub percent level for $k < 1h\text{Mpc}^{-1}$ and the fractional error is generally less than 5 percent even for $k \sim 100h\text{Mpc}^{-1}$. At higher redshift, the fit is still good but shows stronger discrepancies with the interpolation method: in all models, scales and redshifts, the error never exceeds 15 percent for $k < 40h\text{Mpc}^{-1}$, or 33 percent for $k = 100h\text{Mpc}^{-1}$. The fitting formula is accurate to (1, 5, 10) percent at $k = (0.7, 1.5, 20, \text{AGN})$, (1.5, 25, 35, REF) and (1.0, 15, 30, DBLIM), where k is given in $h\text{Mpc}^{-1}$.

Table 2. Best fit parameters that describe the baryonic feedback on the matter power spectrum extracted from the OWL simulations. Given a model m (AGN, REF or DBLIM) and a scale factor $a = 1/(1+z)$, this Table allows the reconstruction of the five terms that enter the baryon feedback bias $b_m(k, z)$ (equations 8 and 10). The index i refers to the power of a associated with the coefficient. For example, the first term is constructed as $A_z = A_2 a^2 + A_1 a + A_0$.

m	i	A_i	B_i	C_i	D_i	E_i
AGN	2	-0.119	0.130	0.600	0.00211	-2.06
	1	0.308	-0.660	-0.760	-0.00295	1.84
	0	0.150	1.22	1.38	0.00130	3.57
REF	2	-0.0588	-0.251	-0.934	-0.00454	0.858
	1	0.0728	0.0381	1.06	0.00652	-1.79
	0	0.00972	1.12	0.750	-0.000196	4.54
DBLIM	2	-0.295	-0.989	-0.0143	0.00199	-0.825
	1	0.490	0.642	-0.0594	-0.00235	-0.0611
	0	-0.0166	1.05	1.30	0.00120	4.48

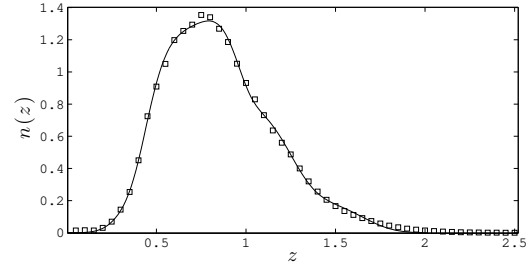


Figure 4. Redshift distribution from CFHTLenS (black squares) corresponding to galaxies with $0.4 < z_{\text{phot}} < 1.3$, with an arbitrary normalization. The solid line is the best fit given by Eq. 11.

3 RESULTS

3.1 Data

We use the public release of the Canada France Hawaii Telescope Lensing Survey (CFHTLenS³) to measure the shear correlation functions ξ_{\pm} . CFHTLenS spans a total survey area of 154 deg^2 , constructed from a mosaic of 171 individual pointings observed by the 1 deg^2 imager at the Canada France Hawaii Telescope. The survey consists of four compact regions called W1, W2, W3 and W4, which cover approximately 64, 23, 44 and 23 deg^2 respectively. Details on the data reduction are described in Erben et al. (2013). The effective area is reduced to 120 deg^2 by the masking of bright stars, artificial and natural moving objects and faulty CCD rows. The observations in the five bands $u'griz$ of the survey allow for the precise measurement of photometric redshifts (Hildebrandt et al. 2012). The shear measurement with *lensfit* is described in detail in Miller et al. (2013). The residual systematics for galaxy shapes are described in Heymans et al. (2012) and the reliability of photometric redshifts is quantified in Benjamin et al. (2013).

As described in Heymans et al. (2012), the star-galaxy shape cross-correlation is the objective criteria, insensitive to cosmology, that is used to flag an individual pointing as *good* or *bad*, depending on its probability to be contaminated by residual Point Spread Function (PSF) distortions. In addition, weak multiplicative and

³ CFHTLenS: www.cfhtlens.org

additive shear calibration factors m and c are calculated and applied; in this work, we revisit the c -correction in order to make it less dependent on an arbitrary parametric model. In Heymans et al. (2012), the c -correction is modelled as a function of the galaxy signal-to-noise v_{SN} and size r , finding an average $\langle c_2 \rangle = 2 \times 10^{-3}$. The additive constant $\langle c_1 \rangle$ was fixed to zero as it was found to be consistent with zero. For this work, it was found that there is also a small dependence on the PSF strelh ratio f_{PSF} previously unaccounted for. In order to compute the new, non-parametric, c -correction, the PSF-corrected galaxy shapes e_1 and e_2 are binned in the three dimensional space $(v_{\text{SN}}, r, f_{\text{PSF}})$, where the statistical shape noise is roughly the same for each cell. In practice, the number of pixels in each dimension is not very important, we verified that the results are unchanged by dividing into 10^3 or 30^3 cells. The c -correction term is obtained by fitting a 3-dimensional third order polynomial for each component e_1 and e_2 . The fitting procedure returns a c_1 and c_2 term as function of the bin position in the $(v_{\text{SN}}, r, f_{\text{PSF}})$ space, which are then assigned to each galaxy. The new c -correction finds that both c_1 and c_2 are non-zero, although on average c_1 is of the order of 5×10^{-4} , still a lot smaller than the average c_2 correction, which averages to 2×10^{-3} as in Heymans et al. (2012). The overall change on the cosmic shear signal between the previous and new c -correction is marginal (i.e. within the noise); the main difference however is a change in the number of *bad* fields. Originally 42 fields were flagged *bad*, while the new c -correction brings this number down to only 24. A further improvement is obtained when the field selection is performed on the same galaxies used for the analysis. Following van Waerbeke et al. (2013) we decided to restrict our analysis to the galaxies with photometric redshifts within $0.4 < z_{\text{phot}} < 1.3$, where the number of z_{phot} outliers and the redshift errors are minimal. The final number of *bad* fields is 14, yielding a total imaging area of 128 deg. sq. of ‘good’ data. The final step is to derive the redshift distribution $n(z)$ for the selected galaxies. As demonstrated in Benjamin et al. (2013), the redshift distribution $n(z)$ is given by the *lensfit*-weighted stacked probability distribution functions of the galaxy sample z_{phot} . In our case, the redshift distribution is well fitted with:

$$n(z) = N_0 e^{-(z-z_0)^4/\sigma_0^2} + N_1 e^{-(z-z_1)^4/\sigma_1^2} + N_2 e^{-(z-z_2)^4/\sigma_2^2} \quad (11)$$

where $(N_0, z_0, \sigma_0, N_1, z_1, \sigma_1, N_2, z_2, \sigma_2) = (0.54828, 0.69972, 0.07412, 0.59666, 0.81567, 0.21624, 0.20735, 1.1337, 0.30801)$. Fig. 4 shows the data and the best fit function. The mean redshift between the two distributions differ by 1.2 percent, which is well below the combined sources of error in our analysis. It is therefore neglected in the rest of the paper.

The shear correlation function measurement follows the same procedure as described in Kilbinger et al. (2013), by averaging over pairs of galaxies:

$$\xi_{\pm}(\theta) = \frac{\sum_{i,j} w_i w_j [e_t(\theta_i) e_t(\theta_j) \pm e_r(\theta_i) e_r(\theta_j)]}{\sum_{i,j} w_i w_j} \quad (12)$$

The sum is performed over all galaxy pairs (i, j) with angular distance $|\theta_i - \theta_j|$ within some bin around θ . The quantities e_t and e_r respectively denote the tangential and cross-component of the galaxy ellipticity. The weights w_i are obtained from the *lensfit* shape measurement pipeline (Miller et al. 2013). This measurement is corrected by the shear calibration factor $1 + K$ given by:

$$1 + K(\theta) = \frac{\sum_{i,j} w_i w_j (1 + m_i)(1 + m_j)}{\sum_{i,j} w_i w_j} \quad (13)$$

The final calibrated measurements are obtained by dividing ξ_{\pm} by

$1 + K$, which is ~ 0.89 for all scales. The error on the calibration on the shear correlation function is completely negligible as shown in Miller et al. (2013).

We also apply a conservative cut on the minimum angular separation for pairs of galaxies. Kilbinger et al. (2013) used 9 arc-seconds which corresponds to the image postage stamp analyzed by *lensfit* (Miller et al. 2013) to measure galaxy shapes. We apply a cut at 20 arc-seconds, which eliminates any possibility of the extended halo of a galaxy pair to be within the same fitted area. The measurement uses the public code ATHENA⁴, and is shown in Fig. 5. The results are divided by the fiducial DM-only model to present the differences between the data and the models. The inner and outer error bars show the statistical and combined statistical and sampling variance uncertainties, respectively.

3.2 Simulations

This work makes use of the two SLICS simulation suites described in HDVW, which are based on WMAP9 + SN + BAO cosmology. The SLICS-LE suite consists of 500 independent N -body realization in which light cones of 60 sq. degrees have been extracted in the multiple thin lens and Born approximations. It achieves better than 10 percent precision for ξ_+ ($\theta > 0.4'$), and down to the few arcminutes for ξ_- ($\theta > 5'$). We use the LE suite to estimate the sampling variance component to the cosmic shear measurement.

The SLICS-HR series is a smaller ensemble of only five light cones in which the resolution is achieved for scales ten times smaller. It serves for convergence assessment and, as mentioned in Section 2.2, as an independent estimate for the dark matter only ξ_+ signal. Details about the measurements of ξ_{\pm} from these two simulation suites are provided in HDVW.

3.3 Theoretical predictions and measurements

3.3.1 Theoretical predictions

Fig. 5 compares a range of model predictions for the real space shear correlation functions $\xi_{\pm}(\theta)$ (obtained with equation 4), with the measurements from the CFHTLenS data. As found by Semboloni et al. (2011), we see that the baryonic feedback alone (thin solid line) tends to suppress the ξ_+ signal at small scales, with very little effect for scales $\theta > 5$ arcminutes, and that the maximum suppression ranges from zero to 20 percent, depending on the model. The neutrino feedback (dashed, dotted and dot-dashed curves) adds an extra suppression that extends over a larger range of angles, exceeding 15 percent even at 100 arcminutes for $M_v \geq 0.4eV$. It is clear from these predictions that non-zero neutrino masses and baryon feedback have similar effects on the weak lensing power spectrum, both leading to power suppression of comparable magnitude.

The combined effect on ξ_- is similar, except that the global shape is shifted to angles ten times larger; this is a simple geometrical effect due to the fact that, for the same angular separation θ , $\xi_-(\theta)$ is probing smaller physical scales than $\xi_+(\theta)$. This could in principle allow for a sensitivity to the positive feedback of stars on the matter power spectrum, which occurs at $\theta < 1$ arcminute; unfortunately this is also in a region where our measurements have the largest error bars, and hence cannot distinguish this feature.

We see from Fig. 5 that both weak lensing shear estimators can

⁴ ATHENA: <http://cosmostat.org/athena.html>

be broken into two zones, separated at the scale where the baryonic feedback starts to have a significant effect; this occurs at $\theta = 5'$ and $40'$ for ξ_+ and ξ_- respectively. The measurement from the ‘large angle’ zone could serve to fix the neutrino mass with minimal contamination from the unknown baryon feedback mechanism, while the small angle zone could constrain (or include a marginalization over) the baryonic feedback model. In this strategy, care must be taken to account for the high level of correlation that exists between the two zones, but this nevertheless could serve as a good starting point for future weak lensing analysis. Note that the exact value of the zone separation angle will change with the source distribution $n(z)$.

We discuss the error bars in the next Section, however we can immediately see from their size that this data cannot distinguish a unique combination of baryon feedback model and neutrino mass. However, certain combinations are unlikely and can even be ruled out with the current data set, given our assumptions on the background cosmology are correct. In particular the dark matter only model seems already disfavoured. Before detailing our model rejection technique (Section 3.5), we first describe our estimate of the full error that enters in this calculation, as this is a very important step for percent precision measurements.

3.4 Error budget

The total error in this measurement comes from the combination of statistical error, sampling variance, modelling error and uncertainty in the background cosmology. Each of these contributions is discussed in this Section.

3.4.1 Statistical

The shape noise generates a statistical error that dominates sampling variance at small scales. It is calculated from the measurement of ξ_{\pm} in 200 noise realizations, where the galaxy orientations extracted from the data have been randomized. The scatter in ξ_{\pm} for each angular bin, and its covariance matrix across bins, is computed for all galaxy pairs that contribute to that particular bin. For the statistical noise, the covariance matrix is almost diagonal and the amplitude of the diagonal elements scale as θ^{-2} .

3.4.2 Sampling variance

The sampling variance is estimated from the LE simulation suite by computing the quantity $\text{Cov}_{N\text{-body}}^{\xi_{\pm}\xi_{\pm}}(\theta, \theta')$. We calculate this quantity for the two auto-correlation ($++$, $--$) terms plus the cross-term ($+-$) in preparation for the combined analysis (see Fig. 6). Since the covariance is inversely proportional to the area, we rescale each of these three quantities by the ratio of the simulation light cones and the CFHTLenS unmasked areas spanned by the good fields (i.e. 60/128) in order to match the sky coverage of the data. We correct for the finite support effect described in HDVW, although this has a sub-percent impact on the sub degree scales under study.

We also include the mixed term arising from the coupling between the shot noise and the sampling variance. We follow the results from Kilbinger et al. (2013) in that the mixed term closely follows the sampling variance term, aside from an overall normalization term taken to be 0.25 and 1.0 for ξ_+ and ξ_- respectively. We verified for the case of ξ_+ that this closely reproduces the analytical calculations described in Schneider et al. (2002), where the effective galaxy densities n_{eff} and the dispersion in the measured

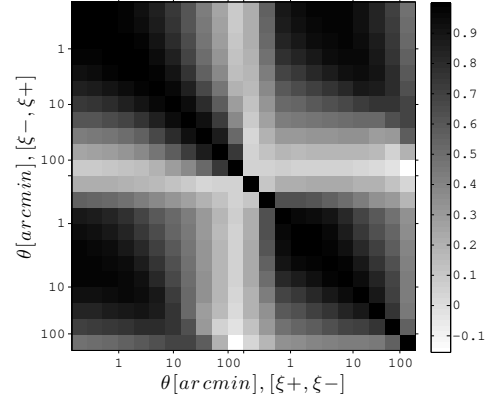


Figure 6. Cross-correlation coefficients about ξ_+ (top left block), ξ_- (bottom right) and the symmetric cross terms (top right and bottom left), measured from the large ensemble of 500 simulations. We recover from the two off-diagonal blocks that the measurements of ξ_- at 10 arcminutes correlate very strongly with those of ξ_+ at 1 arcminute.

galaxy ellipticities σ_{ϵ} are taken to be $n_{\text{eff}} = 9.2 \text{ gal. arcmin}^{-2}$ and $\sigma_{\epsilon} = \sqrt{\sigma_{e1}^2 + \sigma_{e2}^2} = 0.395$, respectively. We report this analytical calculation in Fig. 7 (dotted lines).

We correct for the finite mass resolution in the simulations, a limitation that results in a lack of structure at small scales, causing a drop in both the signal and the covariance. This *missing power* can be quantified by comparisons against reliable prediction models or higher resolution simulations, the SLICS-HR series in this case. The actual impact on the covariance matrix can be estimated from the Hyper Extended Perturbation Theory (Scoccimarro & Friedman 1999), which states that the covariance in power spectrum scales as $\text{Cov}(k, k) \propto P^3(k)$ in the non-linear regime. We therefore use this scaling relation to correct the covariance about $P(k)$, keeping the off-diagonal cross-correlation coefficients fixed, and propagate the effect onto the weak lensing covariance matrix using the Limber approximation (Harnois-Déraps & van Waerbeke in prep.). We show the impact of this correction in Fig. 7 as the red-dashed line. The largest effect is a 10 percent and 200 percent increase in the error about ξ_+ and ξ_- respectively at $\theta < 0.5'$. Above 1 arcmin (ξ_+) and 10 arcmin (ξ_-), the correction is negligible.

The baryonic feedback and neutrino free streaming both suppress the small scale power, which can to some extent be matched to the power loss in the simulations due to mass resolution limits in the N -body calculation. One could then argue that if neutrinos are massive and/or baryon feedback suppresses the matter power in the real Universe, then the mass resolution correction most likely overestimates the error, and the sampling variance computed without this correction is more accurate. This is a valid concern, and should be investigated in the context of future surveys, ideally correcting the covariance in a manner consistent with the model under study. For this work, however, we stay conservative and apply the same correction to all models, keeping in mind that the sampling variance in the case of massive neutrinos and baryon feedback model will be slightly overestimated and hence our constraining power at rejecting these models is slightly too weak.

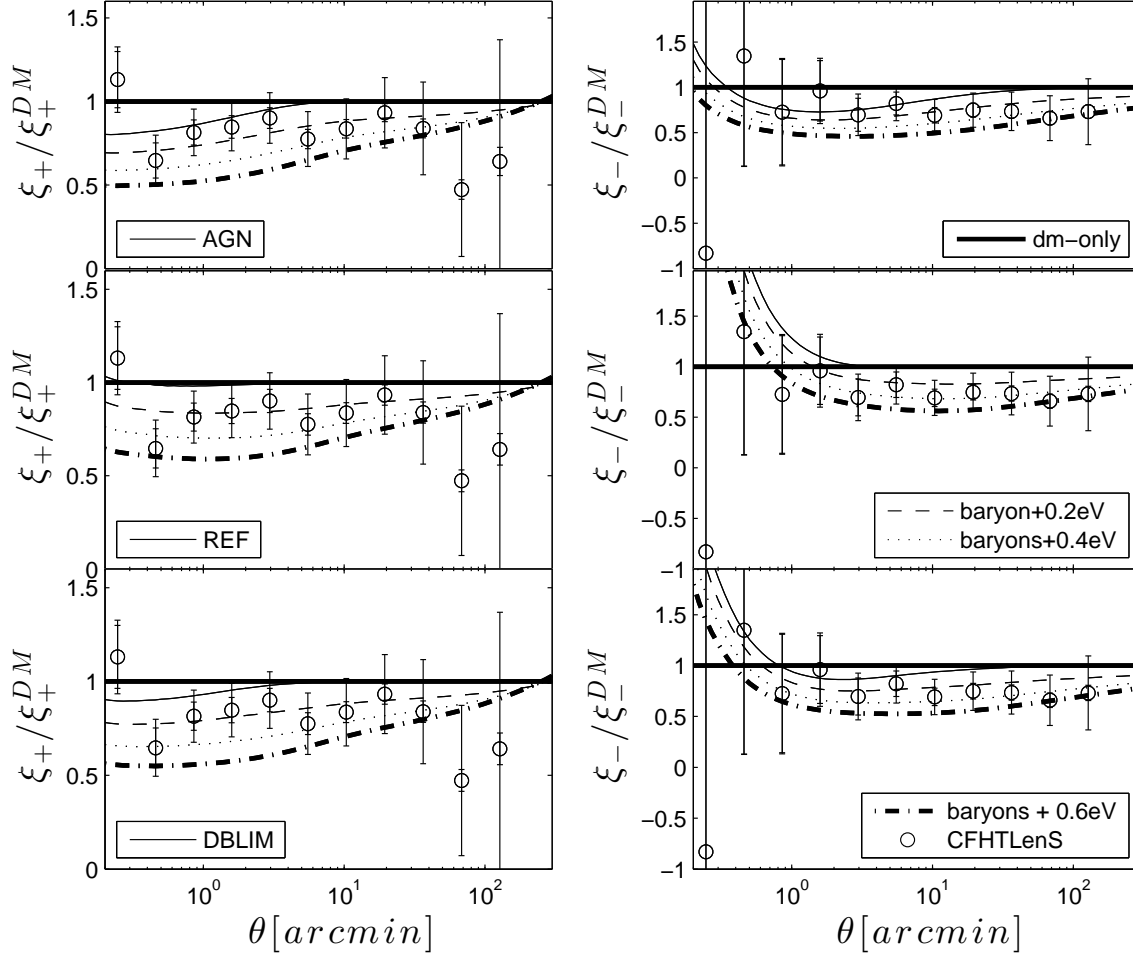


Figure 5. Ratio between all predictions for ξ_{\pm} and the dark matter only model from CEp. Each panel shows the dark matter only model as the thick horizontal line, and the dark matter + baryon model as the thin solid line. Top to bottom are the AGN, REF and DBLIM baryon models respectively. The impact of the neutrinos on each model is shown as the thin dashed lines (0.2eV), dotted lines (0.4eV), and the thick dash-dotted line (0.6eV). The open symbols are the measurements from CFHTLenS, the inner error bars show the statistical error only, while the outer error bar combines all sources of error discussed in Section 3.4.

3.4.3 Non-linear modelling

As discussed in Section 2.2 and observed in Fig. 1, the scatter between the predictions from different pure dark matter non-linear models is always less than five percent for ξ_+ , while it exceeds 50 percent in the smallest angles of ξ_- . Different models and different angles have been weighted by their inverse variance, and the resulting weighted errors on the non-linear models are no more than 4 and 8 percent for ξ_+ and ξ_- respectively (see Section 2.2 for more details). This is treated as a source of systematic uncertainty in our calculation. Comparing this to the other sources of error in Fig. 7, we find this error to be sub-dominant.

3.4.4 Cosmology

In this analysis, we fix the background cosmology to that found by WMAP9+BAO+SN assuming a flat Λ CDM cosmology, in order to probe the impact of neutrinos and baryon feedback. Weak lensing is very sensitive to both the amplitude of the matter power spectrum, characterized either by σ_8 or A_s , and the matter density parameter, Ω_M , with the shear correlation functions scaling roughly

as $\xi_{\pm} \propto \sigma_8 \Omega_M^2 \propto A_s^2 \Omega_M^2$. The WMAP9 constraints on A_s are precise to 3.3 percent, and on Ω_M to 3.4 percent (Hinshaw et al. 2013), and we factor these uncertainties into our analysis through an additional error in our systematic error budget (see dashed, thin lines in Fig. 7). Comparing this ‘cosmological’ uncertainty to the other sources of error in Fig. 7, we find it to be sub-dominant compared to the statistical shot noise (solid, thick) and sampling variance (dashed, thick), as expected from a comparison of cosmological constraint from CFHTLenS data alone (e.g. Kilbinger et al. 2013) with WMAP9. It is however more significant than the uncertainty on the non-linear modelling of the dark matter only signal.

The combined (non-linear model + cosmology) uncertainty on ξ_{\pm} is shown as the error bars about the open circles in Fig. 1. We observe that on small angular scales, both contributions are of the same magnitude, whilst the cosmology errors at large angles are dominant.

3.4.5 Halo sampling variance

Another source of error on the measurement – from both data and simulations – comes from the *halo sampling variance* (HSV here-

after), which is caused by the finiteness of the observation volume. This effect has been studied in terms of the halo model by Sato et al. (2009), which has shown that it can be described by an extra term in the covariance matrix in multipole space:

$$\text{Cov}_{\text{HSV}}(\ell, \ell') = \bar{b}^2 \sigma_{\text{RMS}}^2(\Theta_s) C_\ell^{\kappa, 1h} C_{\ell'}^{\kappa, 1h} \quad (14)$$

where \bar{b}^2 is the mean halo bias, $\sigma_{\text{RMS}}(\Theta_s)$ is the RMS fluctuations in angular clustering inside a circle of area A and radius $\Theta_s = \sqrt{A/\pi}$, and $C_\ell^{\kappa, 1h}$ is the one-halo contribution to the lensing power spectrum, averaged over all halo masses. We propagate this quantity onto our real space weak lensing estimators ξ_\pm as in Joachimi et al. (2008), i.e. using a two-dimensional equivalent of equation 4 and converting $\text{Cov}_{\text{HSV}}(\ell, \ell')$ into $\text{Cov}_{\text{HSV}}^{\xi_\pm}(\theta, \theta')$. We show the contribution to the covariance coming from the HSV in Fig. 7 (dot-dashed), and observe that it is subdominant everywhere. When added in quadrature, it would contribute less than a percent to the total error, hence it can be safely ignored.

3.4.6 Error on the sampling covariance

The residual error in estimates of sampling variance derived from N -body simulations propagate as an *extra error* on the cosmological parameters (Hartlap et al. 2007; Dodelson & Schneider 2013). The size of this error scales as $1 + N_{\text{data}}/N_{\text{sim}}$, i.e. the ratio between the size of the data vector and the number of independent simulations that enter the estimate. In our case, the full data vector (ξ_+ and ξ_- combined) consists of 22 elements, which, when divided by $N_{\text{sim}} = 500$, would contribute a 4 percent error – and two percent for the ξ_+ only measurement – on the precision of cosmological parameters derived from the cosmic shear data. In this analysis, we do not search for cosmological parameters, but instead perform a hypothesis rejection procedure, which is less sensitive to this *extra error* and can therefore be neglected.

3.4.7 Other potential sources of error

The interpretation of the weak lensing signal is in many cases blurred by contamination from secondary effects, the most dominant being the intrinsic alignment that exists between galaxies that are tidally connected. This becomes highly important for analyses based on tomography (Heymans et al. 2013) or full three-dimensional lensing (Kitching et al. 2014), but is a weak effect in our case, owing to the full collapse of the survey along the radial coordinate. We therefore do not include an intrinsic alignment modelling error in our uncertainty. The random error from shape measurements is already absorbed in the statistical error and are therefore not contributing as separate terms. The error on photometric measurement would affect the modelling of the signal via an incorrect estimate of $n(z)$, which would affect the amplitude of the signal. However the uncertainty on this quantity is much smaller than our ‘cosmological’ error and is therefore not included.

3.4.8 The budget

We show the different error contributions to the shear correlation measurements in Fig. 7. The error budget on ξ_+ is dominated by the sampling variance above one arcminute, and by statistical uncertainty at smaller angles. For ξ_- , the statistical error dominates to scales $\theta < 10$ arcminutes with sampling variance dominating at larger scales. Our uncertainty on the background cosmology is at most 50 percent of the sampling variance, while the non-linear

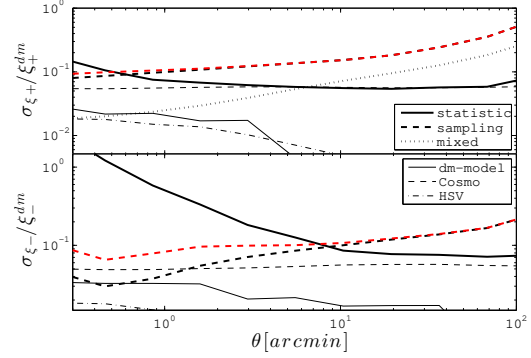


Figure 7. A comparison of the different contributions to the error budget on CFHTLenS measurements of ξ_+ (upper) and ξ_- (lower) as a function of scale. The errors are dominated by statistical shot noise (solid, thick) on small scales and sampling variance (dashed, thick) on large scales. The impact of re-scaling the small angle signal to account for mass resolution effects can be seen by comparing the sampling variance with (red, top) and without (black, bottom) this scaling. The mixed term is shown by the dotted lines (for ξ_+ only) and is smaller than the sampling variance at all scales by at least a factor of 2. For ξ_- , it is taken to be identical to the sampling variance, in good agreement with Kilbinger et al. (2013). By fixing the background cosmology, we include a secondary level error term (dashed, thin) which includes a 3.4 percent uncertainty on Ω_M and a 3.3 percent uncertainty on A_s . The error arising from our uncertainty on the dark matter only non-linear model (solid, thin) is an order of magnitude smaller than the largest error and hence negligible in this measurement. The HSV term (dot-dashed) is sub-dominant everywhere and can be safely ignored.

model uncertainty is sub-dominant at all scales. For both weak lensing quantities, the off-diagonal elements of the covariance are completely dominated by the sampling variance, since the random noise is highly diagonal.

3.5 Model rejection

As discussed by Natarajan et al. (2014), the effects of a non-zero neutrino mass are degenerate with baryonic feedback, particularly at small angular scales. Varying the DM parameters A_s and Ω_M also changes the model on these scales, hence future weak lensing analyses will need to carefully address these degeneracies in the parameter estimations. Although an MCMC analysis would give a complete story, we take here a first step proceeding with a case-by-case model rejection, based on a measurement of the χ^2 for each model and, finally, of the p -value. The p -value captures the statistical significance of the measurement, or, in other words, probability that the data is consistent with the model, *if the model is true*. It is simply given by the integral of the χ^2 probability density function, from the measured χ^2 up to infinity. Lower values represent higher levels of model rejection. Following standard statistics, p -values of (0.317, 0.046, 0.003, ...) correspond to model rejection at the (1σ , 2σ , 3σ , ...) level. This choice of discrimination strategy is driven by the fact that the baryon feedback models are not described by a continuous parameter, meaning that we cannot perform a full likelihood fit to extract a set of baryonic feedback models out of

Table 3. Distribution of p -values for different combination of baryon feedback models and neutrino masses (see main text for details). Specifically, each entry in this Table represents the largest p -value probed inside a $3\sigma_{\text{sys}}$ region about the mean of the model. Values in bold face highlight the model combinations that are excluded by the data with more than 1.64σ significance (p -value < 0.1 , equivalent to a confidence interval (CI) of 90%).

M_ν	ξ_+ alone				ξ_+ and ξ_- combined			
	0.0eV	0.2eV	0.4eV	0.6eV	0.0eV	0.2eV	0.4eV	0.6eV
DM-only	0.036	0.158	0.267	0.230	0.037	0.278	0.621	0.760
AGN	0.110	0.222	0.209	0.120	0.168	0.476	0.659	0.675
REF	0.050	0.189	0.289	0.235	0.030	0.234	0.571	0.728
DBLIM	0.092	0.245	0.283	0.191	0.109	0.438	0.695	0.756

a smooth distribution⁵. Each model is unique and has to be tested independently against the data.

Since we are testing individual models, as opposed to performing a thorough MCMC calculation, it is important to adopt a strategy to account for the three sources of systematic uncertainty – i.e. that on A_s , Ω_M and on the non-linear dark matter only model. We proceed as follows : for each combination of neutrino mass and feedback model, we allow the amplitude of the data signal to vary within a $3\sigma_{\text{sys}}$ range about the measured value and search for the most favourable hypothesis (highest p -value). The systematic uncertainty is maximal at small angles and reaches up to ~ 9 per cent of the model amplitude for both ξ_+ and ξ_- . This means that for our calculation of the p -value, we allow the data points to shift up and down by up to 27% on Fig. 5, keeping the shown error bars (statistical + sampling) fixed. Given that the Planck value for Ω_m is roughly 2σ higher than the WMAP9 best measurement, our $3\sigma_{\text{sys}}$ excursion allows for a nice overlap between both data sets.

Statistically, our model rejection method is equivalent to fitting ($A_s^2\Omega_M^{1.8}$) from the amplitude of the cosmic shear signal, then estimating the neutrino mass for each baryon feedback model from the largest p -value, although our sampling in the M_ν direction has only four points. Accordingly, the number of degrees of freedom must be reduced by two in the conversion between χ^2 and p -values.

We consider two cases, one where the data vector only includes ξ_+ and one with both ξ_+ and ξ_- . The resulting p -values are summarized for all our results in Table 3. The models rejected at more than 1.64σ (i.e. 90% CI) are highlighted in bold. We see that for most ξ_+ models, the p -value is the highest in the 0.4eV column and the smallest in the 0.0eV column, indicating that the preferred value for M_ν is non-zero, although a zero neutrino mass cannot be ruled out. The combined ξ_\pm measurement seems to prefer even higher values of M_ν , but the significance of this statement is weak given the size of the p -values. The dark matter-only model (zero neutrino mass and no baryonic feedback) is however rejected with more than 2σ . It is clear from Fig. 5 that the discriminating power is maximal in the region $\theta < 10$ arcminutes. The combination (REF and massless neutrino) is also excluded at more than 2σ by the data, for having too much power at small angular scales; at the same time, the combination (DBLIM and $M_\nu = 0.0\text{eV}$) is rejected with 91% confidence. Some of the scenarios with massive neutrinos considered here are disfavoured by the ξ_+ data but only with weak significance (88% confidence for the rejection of the AGN feedback model combined with $M_\nu = 0.6\text{eV}$).

Since the first angular bin at $\theta = 0.23$ arcminute is in tension

with the models compared to the other bins, as a sanity check, we explored the impact of excluding that data point, finding no changes on our conclusions, only a modest reduction in the statistical constraining power. This first bin is stable against different minimum separation cuts. As explained in Section 3.2.2, the minimum cut at $\theta_{\text{min}} = 20$ arcsec is very conservative to guarantee that two galaxies do not fall within the same *lensfit* template. In Miller et al. (2013), image simulations showed that the shape of close galaxies were not biased even down to 5 arcseconds separation. We tried various cuts θ_{min} from 5 to 20 arcseconds, and the results shown in Fig. 5 do not change, we are therefore confident that the location of the first bin is robust and not the result of unaccounted residual systematics.

4 DISCUSSION AND CONCLUSION

In this paper, we have considered the use of weak gravitational lensing to probe baryonic feedback and neutrino masses through their effect on the mass power spectrum. For this purpose, we constructed a fitting formula that describes the effect of baryons on the mass power spectrum for three specific models studied in van Daalen et al. (2014). This formula is an analytic function of redshift z and physical scale k , therefore it can be used in cosmological forecasting and MCMC chains, even in the non-linear regime. Our fitting function is highly accurate over the redshift range $0 < z < 1.5$ and scales $k < 100h/\text{Mpc}$, and can be extended to $z = 3$ with a modest degradation in precision at the smallest scales. It can be used for a wide range of cosmological applications, including comparisons between different sets of hydrodynamical simulations, or even high precision baryonic acoustic oscillations measurements (Angulo et al. 2014).

This formula was used to make predictions for the CFHTLenS weak lensing data. We find that the data, in combination with WMAP9 cosmological parameter constraints, reject with *at least* 90% confidence 1) the dark matter only model (i.e. massless neutrinos and no baryon feedback, 96% confidence), 2) the combination of massless neutrinos with baryon feedback model REF (97% confidence), and 3) the combination of baryon feedback model DBLIM with massless neutrinos (91% confidence). These are strong hints that neutrinos are indeed massive, although the massless scenario cannot be completely ruled out in this analysis. The data also disfavours other combinations, although with a lower significance.

Future weak lensing surveys with larger total area will be very promising for this type of analysis, since the CFHTLenS error budget is currently dominated by sampling variance and statistical error. The completed RCS2 survey with its re-analysis RCSLenS⁶ covers close to 700 deg^2 , the ongoing KiDS and HSC will cover

⁵ What we could extract from a MCMC analysis are the preferred values for the parameters of Table 2, but these then need to reconnect with the feedback models, which ultimately resemble the analysis we present in this paper.

⁶ RCSLenS: www.rcslens.org

1500 deg² each, while DES will cover more than 5000 deg². These data sets combined represent a sky area that is ~ 60 times larger than the CFHTLenS survey considered in our study. We show in this paper how we can use the intermediate angle region ($\theta > 5'$ and $40'$ for ξ_+ and ξ_- , respectively) to fix the neutrino mass, then examine and constrain the baryon feedback models with the smaller angles.

Future lensing studies could also probe feedback models as function of galaxy type, age or environment, and study how the density profile of the dark matter halo is affected in a non-uniform manner (Velliscig et al. 2014; Fedeli et al. 2014). Galaxy-galaxy lensing in particular is a promising area where these ideas could be implemented. Cross-correlation studies that are sensitive to feedback effects, such as the cross-correlation between thermal Sunyaev-Zeldovich and gravitational lensing (van Waerbeke et al. 2014; Ma et al. 2014), are also particularly ideal for constraining these models.

It will be interesting to explore whether a tomographic study could help disentangling baryonic feedback from massive neutrinos. One should be careful in that case, however, to take into account intrinsic galaxy alignment, as it is a non-negligible correction to the lensing signal for three redshift bins or more (see Heymans et al. 2013, for example).

Different feedback models are currently given by specific hydrodynamical simulations, but one can envision a not so distant future where it will be possible to implement galactic feedback as just another set of parameters to be simultaneously fit with other cosmological parameters.

ACKNOWLEDGEMENTS

We are deeply grateful to Lance Miller for his essential work on the *good/bad* field selection code and shear calibrations pipelines, and to all the CFHTLenS team for having made public their high quality shear data. We also thank Fergus Simpson and Martin Kilbinger for providing their comments on the draft. Computations for the N -body simulations were performed on the GPC super-computer at the SciNet HPC Consortium. SciNet is funded by: the Canada Foundation for Innovation under the auspices of Compute Canada; the Government of Ontario; Ontario Research Fund - Research Excellence; and the University of Toronto. JHD is supported by a CITA National Fellowship and NSERC, and LvW is funded by the NSERC and Canadian Institute for Advanced Research CIFAR. MV is funded by grant 614.001.103 from the Netherlands Organisation for Scientific Research (NWO). MV and CH acknowledge support from the European Research Council under FP7 grant number 279396 (MV) and 240185 (CH). This work is based on observations obtained with MegaPrime/MegaCam, a joint project of CFHT and CEA/IRFU, at the Canada-France-Hawaii Telescope (CFHT) which is operated by the National Research Council (NRC) of Canada, the Institut National des Sciences de l'Univers of the Centre National de la Recherche Scientifique (CNRS) of France, and the University of Hawaii. This research used the facilities of the Canadian Astronomy Data Centre operated by the National Research Council of Canada with the support of the Canadian Space Agency. CFHTLenS data processing was made possible thanks to significant computing support from the NSERC Research Tools and Instruments grant program.

REFERENCES

- Albrecht, A., Bernstein, G., Cahn, R., et al. 2006, arXiv:astro-ph/0609591
- Angulo, R. E., White, S. D. M., Springel, V. & Henriques, B., 2013, MNRAS, 442, 2131
- Battye, R. A., & Moss, A. 2014, Physical Review Letters, 112, 051303
- Benjamin, J., van Waerbeke, L., Heymans, C., et al. 2013, MNRAS, 431, 1547
- Beutler, F., Saito, S., Brownstein, J. R., et al. 2014, arXiv:1403.4599
- Bird, S., Viel, M., & Haehnelt, M. G. 2012, MNRAS, 420, 2551, 1109.4416
- Cooray, A. R. 1999, A&A, 348, 31
- de Jong, J. T. A., Kuijken, K., Applegate, D., et al. 2013, The Messenger, 154, 44
- Dodelson, S. & Schneider, M. D. .2013, Phys. Rev. D, 88, 063537
- Eifler, T. 2011, MNRAS, 418, 536, 1012.2978
- Eifler, T., Krause, E., Dodelson, S., et al. 2014, arXiv:1405.7423
- Erben, T., Hildebrandt, H., Miller, L., et al. 2013, MNRAS, 433, 2545
- Fedeli, C., Semboloni, E., Velliscig, M., et al. 2014, arXiv:1406.5013
- Fu, L., Kilbinger, M., Erben, T. et al. 2014, arXiv:1404.5469
- Harnois-Deraps, J., & van Waerbeke, L. 2014, ArXiv e-prints, 1406.0543
- Hartlap, J., Simon, P. and Schneider, P. 2007, A&A, 464, 399
- Heitmann, K., Lawrence, E., Kwan, J., Habib, S., & Higdon, D. 2013, ArXiv e-prints, 1304.7849
- Heitmann, K., White, M., Wagner, C., Habib, S., & Higdon, D. 2010, ApJ, 715, 104
- Heymans, C., Groucutt, E., Heavens, A. F. et al. 2013, MNRAS, 432, 2433
- Heymans, C., van Waerbeke, L., Miller, L., et al. 2012, MNRAS, 427, 146
- Hildebrandt, H., Erben, T., Kuijken, K., et al. 2012, MNRAS, 421, 2355
- Hinshaw, G., Larson, D., Komatsu, E., et al. 2013, ApJ, 208, 19
- Joachimi, B., Schneider, P. and Eifler, T. 2008, A&A, 477, 43
- Kilbinger, M., Fu, L., Heymans, C., et al. 2013, MNRAS, 430, 2200
- Kitching, T. D., Heavens, A. F., Alsing, J., et al. 2014, MNRAS, 442, 1326
- Lewis, A., Challinor, A., & Lasenby, A. 2000, Astrophys. J., 538, 473
- Limber, D. N. 1954, ApJ, 119, 655
- Ma, Y.-Z., van Waerbeke, L., Hinshaw, G., Hojjati, A., & Scott, D. 2014, arXiv:1404.4808
- Mandelbaum, R., Rowe, B., Bosch, J., et al. 2014, ApJS, 212, 5
- Miller, L., Heymans, C., Kitching, T. D., et al. 2013, MNRAS, 429, 2858
- Natarajan, A., Zentner, A. R., Battaglia, N., & Trac, H. 2014, ArXiv e-prints, 1405.6205
- Planck Collaboration et al. 2013, ArXiv e-prints, 1303.5076
- Riemer-Sorensen, S., Blake, C., Parkinson, D., et al. 2012, Phys. Rev. D, 85, 081101
- Rossi, G. 2014, arXiv:1406.5411
- Sánchez, E., & DES Collaboration 2014, arXiv:1406.4407S
- Sato, M., Hamana T., Takahashi, R. et al. 2009, ApJ, 701, 945
- Schaye, J. et al. 2010, MNRAS, 402, 1536, 0909.5196
- Schneider, P., van Waerbeke L., Kilbinger, M. and Mellier, Y.

- 2002, *A&A*, 396, 1
- Scoccimaro, R. & Friedman 1999, *ApJ*, 520, 35
- Semboloni, E., Hoekstra, H., Schaye, J., van Daalen, M. P., & McCarthy, I. G. 2011, *MNRAS*, 417, 2020
- Simpson, F., Heymans, C., Parkinson, D. et al. 2013, *MNRAS*, 429, 2249
- Smith, R. E. et al. 2003, *MNRAS*, 341, 1311
- Takahashi, R., Sato, M., Nishimichi, T., Taruya, A., & Oguri, M. 2012, *ApJ*, 761, 152
- van Daalen, M. P., Schaye, J., McCarthy, I. G., Booth, C. M., & Vecchia, C. D. 2014, *MNRAS*, 440, 2997
- van Daalen, M. P., Schaye, J., Booth, C. M., & Dalla Vecchia, C. 2011, *MNRAS*, 415, 3649, 1104.1174
- van Waerbeke, L., Benjamin, J., Erben, T. et al. 2013, *MNRAS*, 433, 3373
- van Waerbeke, L., Hinshaw, G., & Murray, N. 2014, *Phys. Rev. D*, 89, 023508
- Velliscig, M., van Daalen, M. P., Schaye, J., McCarthy, I. G., Cacciato, M., LeBrun, A. M. C. & Vecchia, C. D. 2014, *MNRAS*, 442, 2641
- Weinberg, D. Mortonson, M. Eisenstein, D. et al. 2013, *Phys. Rep.*, 530, 87.
- Zhao, G.-B., Saito, S., Percival, W. J., et al. 2013, *MNRAS*, 436, 2038

This paper has been typeset from a $\text{\TeX}/\text{\LaTeX}$ file prepared by the author.